Supporting Information for "Exploring Antarctic feedback mechanisms using two-way coupled subglacial hydrology and ice flow modeling in the Siple Coast"

Koi McArthur[1], Christine Dow[1,2], Shivani Ehrenfeucht[2,3]

[1]Department of Applied Mathematics, University of Waterloo, Waterloo, ON, Canada

[2]Department of Geography and Environmental Management, University of Waterloo, Waterloo, ON, Canada

[3]Potsdam Institute for Climate Impact Research, Potsdam, Germany

Contents of this file

1. Text S1 to S6
2. Figures S1 to S3
3. Table S1

Introduction

The supporting information for "Exploring Antarctic feedback mechanisms using two-way coupled subglacial hydrology and ice flow modeling in the Siple Coast" consists of Text S1 through S7, Figures S1 through S3, and Table S1. Text S1 discusses changes to the GlaDS sheet equations. Text S2 discusses the additional coupling components: including subglacial lake geometry in the driving stress of the stress balance model, and temporally variable basal melt input due to geothermal heat flux and frictional melting of

ice. Text S3 discusses the computational mesh for the models and timestepping. Text S4 discusses boundary conditions used in the models. Text S5 discusses the friction law used in the ice flow and coupled models. Text S6 goes through the initialization procedure for the ice flow and coupled models. Text S7 contains a GlaDS sensitivity test to the sheet conductivity. Figure S1 is a schematic of the coupled model. Figure S2 shows the impact of the coupling strength constant on the motion of Ice Stream B. Figure S3 compares flotation fraction from steady-state hydrology models with various sheet conductivities. Table S1 contains all relevant modeling parameters.

Text S1 - GlaDS sheet equations

The hydrology sheet in GlaDS evolves as

$$\frac{\partial h}{\partial t} = \omega_s - \nu_s, \tag{1}$$

$$\omega_s = \begin{cases} u_b(h_r - h)/\ell_r, & h < h_r \\ 0, & h \geq h_r \end{cases}, \tag{2}$$

$$\nu_s = Ah\,|N|^{n-1}\,N, \tag{3}$$

$$N = \begin{cases} \phi_0 - \phi + \rho_w g h, & h < h_c \\ \phi_0 - \phi + \rho_w g h \cdot \exp\left(\gamma(\frac{h-h_c}{h_c})\right), & h \geq h_c \end{cases}, \tag{4}$$

where h is the hydrology sheet thickness, ω_s is the hydrology sheet opening rate, ν_s is the hydrology sheet closing rate, u_b is the basal ice speed, h_r is the typical bedrock bump height, ℓ_r is the typical cavity spacing, A is the ice rheological constant (not to be confused with the ice rheological parameter used in the stress balance equations) corresponding to ice at -2 °C (approximately pressure melting point) multiplied by an order one factor

related to the cavity/channel geometry, N is the effective pressure, ϕ_0 is the overburden hydraulic potential, ϕ is the hydraulic potential, ρ_w is the density of fresh water, g is the gravitational acceleration, and h_c and γ are constants controlling the growth of subglacial lakes. When $h \geq h_r$, as is the case with subglacial lakes, the hydrology sheet can only open due to the creep closure term ν_s (if $N < 0$). This does not represent the physical processes involved in changes in subglacial lake depth, but it is necessary in order to have evolving lakes in GlaDS in the absence of specialized lake equations. Therefore, lakes in GlaDS fill to a depth such that $N = 0$. Unlike in Werder et al. (2013), we calculate the effective pressure at the ice/water interface (for $h < h_c$), not at the glacier bed. To avoid unrealistically deep lakes we alter the calculation of the effective pressure for $h \geq h_c$, where $h_c > h_r$. This will deliberately underestimate water pressure at the lake/ice interface, resulting in a shallower lake. Smaller values of h_c, will lead to shallower lakes, and smaller impacts on glacier driving stress. For this study we chose a value of $h_c = 10\,\mathrm{m}$ in the transient simulations, consistent with final modeled lake depths under Ice Stream B in Model-H. A common approach to limiting the growth of subglacial hydrologic features is the application of a hard cap. GlaDS caps the maximum channel area and ISSM-SHAKTI (Sommers et al., 2018) caps the sheet thickness. Using such an approach in this study would mean that it would be more difficult to investigate the impact of subglacial lake geometry altering glacier driving stress. Runaway channel growth in GlaDS and runaway sheet growth in SHAKTI are due to the inclusion of melt from dissipation of potential energy. Since sliding as opposed to melt is the dominant cavity opening mechanism (Walder, 1986; Kamb, 1987) we only include melt due to dissipation of potential energy

in the channel system, which is unaltered from Werder et al. (2013). A description of the full GlaDS equations is given in Werder et al. (2013).

Text S2 - Additional coupling components

The Shallow Shelf Approximation (MacAyeal, 1989, SSA) is given by

$$\frac{\partial}{\partial x}\left(4H\bar{\mu}\frac{\partial u}{\partial x}+2H\bar{\mu}\frac{\partial v}{\partial y}\right)+\frac{\partial}{\partial y}\left(H\bar{\mu}\frac{\partial u}{\partial y}+H\bar{\mu}\frac{\partial v}{\partial x}\right)+\tau_{b,x}=\rho_i g H\frac{\partial S}{\partial x}$$
$$\frac{\partial}{\partial y}\left(4H\bar{\mu}\frac{\partial v}{\partial y}+2H\bar{\mu}\frac{\partial u}{\partial x}\right)+\frac{\partial}{\partial x}\left(H\bar{\mu}\frac{\partial u}{\partial y}+H\bar{\mu}\frac{\partial v}{\partial x}\right)+\tau_{b,y}=\rho_i g H\frac{\partial S}{\partial y}, \quad (5)$$

where $\bar{\mu}$ is the depth averaged viscosity, H is the ice thickness, τ_{bx} and τ_{by} are the x and y components of the basal shear stress respectively, S is the ice surface elevation, and v_x and v_y are the x and y components of the velocity respectively. On the left hand side, the first term is compressional/extensional motion, the second term is shear motion, and the third term is basal shear stress. These three terms act to balance the driving stress, which is on the right hand side of the equations. We modify Eq. (5) to include the effects of subglacial lakes in the driving stress term as

$$\frac{\partial}{\partial x}\left(4H\bar{\mu}\frac{\partial u}{\partial x}+2H\bar{\mu}\frac{\partial v}{\partial y}\right)+\frac{\partial}{\partial y}\left(H\bar{\mu}\frac{\partial u}{\partial y}+H\bar{\mu}\frac{\partial v}{\partial x}\right)+\tau_{b,x}=\rho_i g H\frac{\partial}{\partial x}(S+h_\ell)$$
$$\frac{\partial}{\partial y}\left(4H\bar{\mu}\frac{\partial v}{\partial y}+2H\bar{\mu}\frac{\partial u}{\partial x}\right)+\frac{\partial}{\partial x}\left(H\bar{\mu}\frac{\partial u}{\partial y}+H\bar{\mu}\frac{\partial v}{\partial x}\right)+\tau_{b,y}=\rho_i g H\frac{\partial}{\partial y}(S+h_\ell), \quad (6)$$

$$h_\ell=\begin{cases}0 & h\le h_r\\ h-h_r & h>h_r\end{cases}, \quad (7)$$

where h_ℓ is the thickness of the hydrology sheet above the typical bedrock bump height. We assume that the ice surface is instantaneously uplifted by the subglacial lake depth

(h_ℓ), whereas in reality, lakes would result in flexure and a viscous response of the ice sheet.

The temporally variable melt rate is calculated by

$$m_s = \frac{G + \tau_b u_b}{\rho_i L}, \tag{8}$$

where m_s is the melt water input to the linked cavity system, G is the geothermal heat flux, ρ_i is the density of ice, and L is the latent heat of melting.

In all coupled models the ice speed from the ice flow model is input into the hydrology sheet opening rate in GlaDS, the ice geometry from the ice flow model is used to calculate the overburden hydraulic potential whenever the effective pressure is calculated in GlaDS, and the effective pressure from GlaDS is used in the friction law of the ice flow model. A schematic of the coupling process is given in Fig. S1.

Text S3 - Computational mesh

All hydrology, ice flow, and coupled models are run over the Ross Sea subglacial hydrologic catchment, calculated assuming overburden hydraulic potential. The computational mesh consists of 429316 elements with a minimum edge length of 225 m. The mesh has a typical edge length of 10 km but is refined in areas of fast ice motion ($> 100\,\mathrm{m\,year^{-1}}$), near the troughs draining through the Transantarctic Mountains, and in the Ross Ice Shelf to have a typical edge length of 2 km.

GlaDS has 0.5 day timestepping in all models, the ice-flow only models have 1 day timestepping, and the coupled models have 2 week timestepping in the mass transport model.

The thermal model discussed in Text S5 has a computational mesh with 596116 elements and 5 vertical layers with an extrusion exponent of 1. The ice temperature is depth averaged at each horizontal vertex and interpolated onto the computational mesh of the hydrology/ice flow/coupled models to use to calculate ice rigidity over the grounded domain for the ice flow and coupled models.

Text S4 - Boundary conditions Dirichlet boundary conditions of ice surface velocity from MEaSUREs v2 Rignot et al. (2017) and ice thickness from BedMachine Antarctica v3.4 Morlighem et al. (2020) are applied at the domain boundary in the stress balance and mass transport models respectively. In the coupled models, an outflow Neumann boundary condition of $-10^{-4}\,\mathrm{m^2\,s^{-1}}$ is applied in GlaDS at the domain boundary, to allow water to drain from the domain as the glacier geometry changes. In Model-H, a zero flux boundary condition is applied at the catchment boundary. In all GlaDS models a Dirichlet boundary condition of overburden hydraulic potential is applied at the grounding line.

Text S5 - Friction law

Basal friction is calculated using a regularized Coulomb friction law (Schoof, 2005; Gagliardini et al., 2007) that we modify so that the basal shear stress responds to changes in effective pressure and ice speed in a way that is consistent with subglacial conditions predicted from GlaDS. We refer to this friction law as the "hydrology-modified Schoof friction law" and it is given by

$$\boldsymbol{\tau_b} = \frac{C^2 \mid \boldsymbol{u_b} \mid^{m-1}}{(1 + (\zeta/N)^{1/m} \mid \boldsymbol{u_b} \mid)^m} \boldsymbol{u_b}, \tag{9}$$

where $\boldsymbol{\tau_b}$ is the basal shear stress, N is the effective pressure, C is the hydrology-modified Schoof friction coefficient, ζ is the coupling strength constant (discussed below), $|\,\boldsymbol{u_b}\,|$ is the basal ice speed, which in the SSA is the depth averaged ice speed, and $m = 1/n$, where $n = 3$ is the exponent in Glen's flow law (Glen & Perutz, 1955). This is the same as a regularized Coulomb friction law that is commonly known as the "Schoof friction law" up to a renaming of model parameters. The Schoof friction law is given by

$$\boldsymbol{\tau_b} = \frac{C_s^2 \left|\boldsymbol{u_b}\right|^{m-1}}{(1 + (C_s^2/(C_{\max}N))^{1/m} \left|\boldsymbol{u_b}\right|)^m} \boldsymbol{u_b}, \tag{10}$$

where C_s is the Schoof friction coefficient and $C_{\max}$ is Iken's bound. There is a dimensionless variable in the denominator of the Schoof and hydrology-modified Schoof friction laws that we refer to as the "sliding regime" of the friction law. For the Schoof friction law the sliding regime is given by $\xi = (C_s^2/(C_{\max}N))^{1/m} \left|\boldsymbol{u_b}\right|$. When $\xi << 1$ then $\tau_b \approx C_s^2 u_b^m$. The friction law behaves like the Weertman sliding law, or is in a "Weertman sliding regime." When $\xi >> 1$ then $\tau_b \approx C_{\max}N$ and the basal shear stress is determined by Iken's bound, or is in an "Iken sliding regime." We want the behavior of the friction law to be consistent with subglacial conditions related to basal sliding predicted from GlaDS. A good proxy for this is

$$\theta = \begin{cases} h/h_r & h < h_r \\ 1 & h \geq h_r \end{cases}, \tag{11}$$

which we call "the degree of cavitation." If $\theta \approx 0$ then there is minimal sliding over subglacial cavities and when $\theta \approx 1$ then the glacier is losing contact with the bed and there would be sliding over water filled cavities. For the friction law to be consistent with subglacial conditions predicted from GlaDS, we want ξ to be a monotonically increasing

function of θ that goes to 0 when θ goes to 0 and goes to ∞ when θ goes to 1. For $\theta < 1$ in steady state Eq. (1) gives us

$$\frac{u_b}{N^n} = \frac{A\theta\ell_r}{1-\theta}, \tag{12}$$

where u_b is the basal sliding speed. So, u_b/N^n is a monotonically increasing function of θ that goes to 0 as θ goes to 0 and goes to ∞ as θ goes to 1 (A and ℓ_r are spatially uniform in GlaDS). When using regularized Coulomb friction laws on real domains, the friction coefficient is usually determined from inverse methods by matching simulated and observed ice surface velocity, while Iken's bound is held spatially uniform. This means that $C_s^2/C_{\max}$ varies spatially and ξ will not be a monotonically increasing function of θ. However, if we set $C_s^2/C_{\max}$ to be spatially uniform, then ξ will be a monotonically increasing function of θ, it will go to 0 as θ goes to 0, and it will go to ∞ as θ goes to 1. The friction law will be consistent with subglacial conditions related to basal sliding, predicted by GlaDS.

We explicitly rename $C_s^2/C_{\max}$ as the coupling strength constant (ζ) and keep ζ spatially uniform in the hydrology-modified Schoof friction law. This ensures that the sliding regime of the friction law is spatially consistent with the degree of cavitation at the glacier bed. Now, when C is determined using inverse methods, the value of $C_{\max} = C^2/\zeta$ will simultaneously be determined. We also note that since $\zeta = C_s^2/C_{\max}$, ζ can be thought of as the ratio of a parameter describing bed roughness to Iken's bound (the maximum angle on the stoss face of bedrock obstacles).

The grounding line is determined from a flotation criteria, in elements that are partially grounded and partially floating, the friction determined from the hydrology-modified

Schoof friction law is multiplied by the fraction of grounded area in the element. In elements that are fully floating, no friction is applied.

To test the sensitivity of the hydrology-modified Schoof friction law to the value of ζ we run our coupled models with the new value of $\zeta = 2 \cdot 10^7\,\mathrm{m^{-4}\,kg\,s}$, the value of $\zeta = 10^7\,\mathrm{m^{-4}\,kg\,s}$ was used in the main text. The models with the new value of $\zeta = 2 \cdot 10^7\,\mathrm{m^{-4}\,kg\,s}$ are denoted Model-C2, Model-C2-control, Model-CM2, Model-CD2, and Model-CF2. Increasing ζ increased the size of the pulses of ice motion in ice streams B and D by nearly a factor of 4, and reduced the ice speed variability in Ice Stream B over the first half of the simulation in Model-CM2 compared to Model-C2 (Fig. S3). The pulses in ice motion in the models with larger ζ have amplitude larger than expected in the Siple Coast region, for the given timescales of the pulse. Therefore the lower ζ models are presented in the main paper.

Text S6 - Initialization procedure

To approximate the condition of the subglacial hydrologic system and the ice sheet in 2010 (the start date for the ice flow and coupled models), we use an initialization procedure involving inversions for the basal friction coefficient and ice rigidity, steady state hydrology runs, and relaxation ice flow runs. Using the effective pressure from Model-H we run a series of four inversions: 1) we invert for the ice rigidity over the floating domain; 2) using the Budd friction law (Budd et al., 1979) we invert for the Budd friction coefficient over the grounded domain; 3) we invert for the ice rigidity over the floating domain; 4) we convert to the hydrology-modified Schoof friction law (Text S4) and invert for the friction coefficient over the grounded domain. We then run a 20 year ice flow relaxation, invert for the ice rigidity over the entire domain and the basal friction coefficient over

the grounded domain using the updated ice geometry, and then rerun the 20 year ice flow relaxation using the ice rigidity and basal friction coefficient from those inversions. The ice geometry and speed from the second ice flow relaxation are used to run a hydrology model relaxation for 70 years with a switch from $h_c = 100\,\mathrm{m}$ to $h_c = 10\,\mathrm{m}$ at 50 years. For Model-CM and Model-CF the variable melt rate is applied during this hydrology relaxation. With the effective pressure from the hydrology relaxation, the basal friction coefficient is calculated assuming the same basal shear stress at the end of the ice flow relaxation. Finally, there are two last inversions for the ice rigidity over the entire domain and the basal friction coefficient over the grounded domain, and a 1 year relaxation of the model with all appropriate components activated.

The switch to $h_c = 10\,\mathrm{m}$ during the hydrology relaxation is to ensure that lakes don't become unrealistically deep in the coupled models. This switch was made at 50 years to allow the model to adjust to the change in ice geometry separately to the change in h_c. Since this is a relaxation to near steady state, making the switch at an earlier point in the simulation is unlikely to have a large impact on the final timestep of the model.

Each inversion minimizes a cost function with an absolute velocity misfit term ($\mathcal{J}_a$), a logarithmic velocity misfit term ($\mathcal{J}_l$), and a Tikhonov regularization term ($\mathcal{J}_r$). The absolute velocity misfit term ensures a good velocity match in fast flowing regions, the logarithmic velocity misfit term ensures a good velocity match in slow flowing regions, and the Tikhonov regularization term ensures that gradients in ice rigidity and the basal friction coefficient do not become too large (close by elements should have similar friction and rigidity properties). The terms making up the cost function are multiplied by "cost function coefficients" that control the importance of each term in the cost function. These

coefficients are chosen so that the velocity misfit terms are on the same order of magnitude, which is approximately $10^2 - 10^3$, and the regularization term is two orders of magnitude smaller than the velocity misfit terms. The absolute velocity misfit term is given by

$$\mathcal{J}_{\mathrm{a}}(\boldsymbol{u}) = \alpha_a \iint_{\Sigma} \frac{1}{2} \left(\left(u - u^{\mathrm{obs}}\right)^2 + \left(v - v^{\mathrm{obs}}\right)^2 \right) d\Sigma, \tag{13}$$

where $\boldsymbol{u}$ is the ice velocity, u and v are the x and y components of ice velocity respectively, u^{obs} and v^{obs} are the x and y components of the observed ice velocity from MEaSUREs v2 (Rignot et al., 2011, 2017; Mouginot et al., 2012, 2017) respectively, α_a is the cost function coefficient for the absolute velocity misfit term, and Σ is the two dimensional domain. $\mathcal{J}_l$ is given by

$$\mathcal{J}_{\mathrm{l}}(\boldsymbol{u}) = \alpha_l \iint_{\Sigma} \left(\log \left(\frac{||\boldsymbol{u}|| + \varepsilon}{||\boldsymbol{u}^{\mathrm{obs}}|| + \varepsilon} \right) \right)^2 d\Sigma, \tag{14}$$

where $\boldsymbol{u}^{\mathrm{obs}}$ is the observed ice velocity from MEaSUREs v2 (Rignot et al., 2017), α_l is the cost function coefficient for the logarithmic velocity misfit term, and ε is a small constant close to machine precision to avoid division by 0 when the observed ice speed is 0. $\mathcal{J}_r$ is given by

$$\mathcal{J}_{\mathrm{r}}(\boldsymbol{u}) = \alpha_r \iint_{\Sigma} \frac{1}{2} \left| \boldsymbol{\nabla} \kappa \right|^2 d\Sigma, \tag{15}$$

where κ is the variable being inverted for, which is the ice rigidity or the basal friction coefficient, and α_r is the cost function coefficient for the regularization term. The total cost function is given by

$$\mathcal{J} = \mathcal{J}_{\mathrm{a}} + \mathcal{J}_{\mathrm{l}} + \mathcal{J}_{\mathrm{t}}, \tag{16}$$

Text S7 - Sheet conductivity sensitivity

GlaDS has a history of use in Antarctica (C. Dow et al., 2020; C. F. Dow et al., 2022; McArthur et al., 2023; Pelle et al., 2024; Ehrenfeucht et al., 2025) and most model parameters remain very similar across these studies. Since GlaDS has many model parameters it can be difficult to decide on the best parameters to use for any given study. For this reason the sheet and channel conductivities are typically varied (Werder et al., 2013; C. Dow et al., 2020) to produce realistic effective pressure, while the other parameters are held constant. We run steady-state GlaDS with alternative values of the sheet conductivity ($k_s = 10^{-4}\,\mathrm{m}^{7/4}\,\mathrm{kg}^{-1/2}$, and $k_s = 5 \cdot 10^{-3}\,\mathrm{m}^{7/4}\,\mathrm{kg}^{-1/2}$) and plot the effective pressure from these models along with the effective pressure from Model-H in Fig. S3. Increasing the sheet conductivity reduces flotation fraction so that much of the domain is below a flotation fraction of 0.8, and reducing the sheet conductivity raises the flotation fraction so that much of the domain is nearly at flotation.

References

Budd, W. F., Keage, P. L., & Blundy, N. A. (1979). Empirical Studies of Ice Sliding. , *23*(89), 157–170. doi: 10.3189/S0022143000029804

Dow, C., McCormack, F., Young, D., Greenbaum, J., Roberts, J., & Blankenship, D. (2020). Totten Glacier subglacial hydrology determined from geophysics and modeling. *Earth and planetary science letters*, *531*, 115961-. doi: https://doi.org/10.1016/j.epsl.2019.115961

Dow, C. F., Ross, N., Jeofry, H., Siu, K., & Siegert, M. J. (2022). Antarctic basal environment shaped by high-pressure flow through a subglacial river system. *Nature geoscience*, *15*(11), 892-898. doi: https://doi-org.proxy.lib.uwaterloo.ca/10.1038/

s41561-022-01059-1

Ehrenfeucht, S., Dow, C., McArthur, K., Morlighem, M., & McCormack, F. S. (2025). Antarctic Wide Subglacial Hydrology Modeling. *Geophysical research letters*, *52*(1). doi: https://doi-org.proxy.lib.uwaterloo.ca/10.1029/2024GL111386

Gagliardini, O., Cohen, D., Råback, P., & Zwinger, T. (2007). Finite-element modeling of subglacial cavities and related friction law. *Journal of Geophysical Research*, *112*(F2), F02027.

Glen, J. W., & Perutz, M. F. (1955). The creep of polycrystalline ice. *Proceedings of the Royal Society of London. Series A. Mathematical and Physical Sciences*, *228*(1175), 519-538. Retrieved from `https://royalsocietypublishing.org/doi/abs/10.1098/rspa.1955.0066` doi: 10.1098/rspa.1955.0066

Kamb, B. (1987). Glacier surge mechanism based on linked cavity configuration of the basal water conduit system. *J. of Geophys. Res.: Solid Earth*, *92*(B9), 9083-9100. Retrieved from `https://agupubs.onlinelibrary.wiley.com/doi/abs/10.1029/JB092iB09p09083` doi: https://doi.org/10.1029/JB092iB09p09083

MacAyeal, D. R. (1989). Large-scale ice flow over a viscous basal sediment: Theory and application to ice stream B, Antarctica. *Journal of Geophysical Research*, *94*(B4), 4071-4087.

McArthur, K., McCormack, F. S., & Dow, C. F. (2023). Basal conditions of Denman Glacier from glacier hydrology and ice dynamics modeling. *The Cryosphere*, *17*(11), 4705–4727. Retrieved from `https://tc.copernicus.org/articles/17/4705/2023/` doi: 10.5194/tc-17-4705-2023

Morlighem, M., Rignot, E., Binder, T., Blankenship, D., Drews, R., Eagles, G., ...

others (2020). Deep Glacial Troughs and Stabilizing Ridges Unveiled beneath the Margins of the Antarctic Ice Sheet. *Nature Geoscience*, *13*, 132–137. doi: 10.1038/s41561-019-0510-8

Mouginot, J., Rignot, E., Scheuchl, B., & Millan, R. (2017). Comprehensive Annual Ice Sheet Velocity Mapping Using Landsat-8, Sentinel-1, and RADARSAT-2 Data. *Remote Sensing*, *9*(4), 364.

Mouginot, J., Scheuchl, B., & Rignot, E. (2012). Mapping of Ice Motion in Antarctica Using Synthetic-Aperture Radar Data. *Remote Sensing*, *4*(9), 2753-2767.

Pelle, T., Greenbaum, J. S., Ehrenfeucht, S., Dow, C. F., & McCormack, F. S. (2024). Subglacial Discharge Accelerates Dynamic Retreat of Aurora Subglacial Basin Outlet Glaciers, East Antarctica, Over the 21st Century. *Journal of geophysical research. Earth surface*, *129*(7).

Rignot, E., Mouginot, J., & Scheuchl, B. (2011, September). Ice Flow of the Antarctic Ice Sheet [Article]. *Science*, *333*(6048), 1427–1430. doi: 10.1126/science.1208336

Rignot, E., Mouginot, J., & Scheuchl, B. (2017). *MEaSUREs InSAR-Based Antarctica Ice Velocity Map, Version 2 [Data Set]. Boulder, Colorado USA. NASA National Snow and Ice Data Center Distributed Active Archive Center.* (Accessed 06-10-2021.) doi: https://doi.org/10.5067/D7GK8F5J8M8R

Schoof, C. (2005). The effect of cavitation on glacier sliding. *Proceedings of the Royal Society. A, Mathematical, Physical, and Engineering Sciences*, *461*(2055), 609-627.

Sommers, A., Rajaram, H., & Morlighem, M. (2018). SHAKTI: Subglacial Hydrology and Kinetic, Transient Interactions v1.0. *Geoscientific Model Development*, *11*(7), 2955–2974. Retrieved from `https://gmd.copernicus.org/articles/11/2955/2018/` doi:

10.5194/gmd-11-2955-2018

Walder, J. S. (1986). Hydraulics of Subglacial Cavities. , *32*(112), 439–445. doi: 10.3189/S0022143000012156

Werder, M. A., Hewitt, I. J., Schoof, C. G., & Flowers, G. E. (2013). Modeling Channelized and Distributed Subglacial Drainage in Two Dimensions. *Journal of Geophysical Research*, *118*, 2140–2158. doi: doi:10.1002/jgrf.20146,

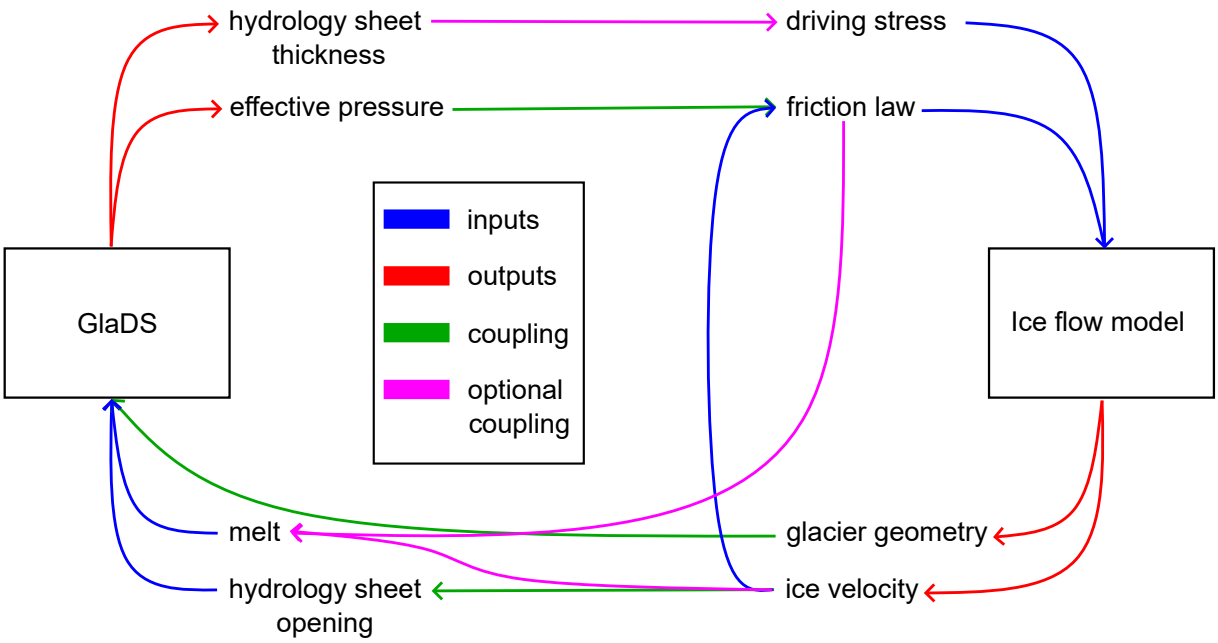


Figure S1. Schematic of the coupling between GlaDS and the ice flow model. Model inputs are represented by blue lines; model outputs are represented by red lines; green lines represent model outputs which are always fed as model inputs during coupling; pink lines represent model outputs which can be fed as model inputs during coupling with variable melt or the inclusion of subglacial lake geometry in the driving stress calculation. Outputs from GlaDS that are fed back into GlaDS and outputs from the ice flow model that are fed back into the ice flow model are not depicted in the figure, except ice velocity, which is fed into the friction law and used in the calculation of the variable melt rate in GlaDS.

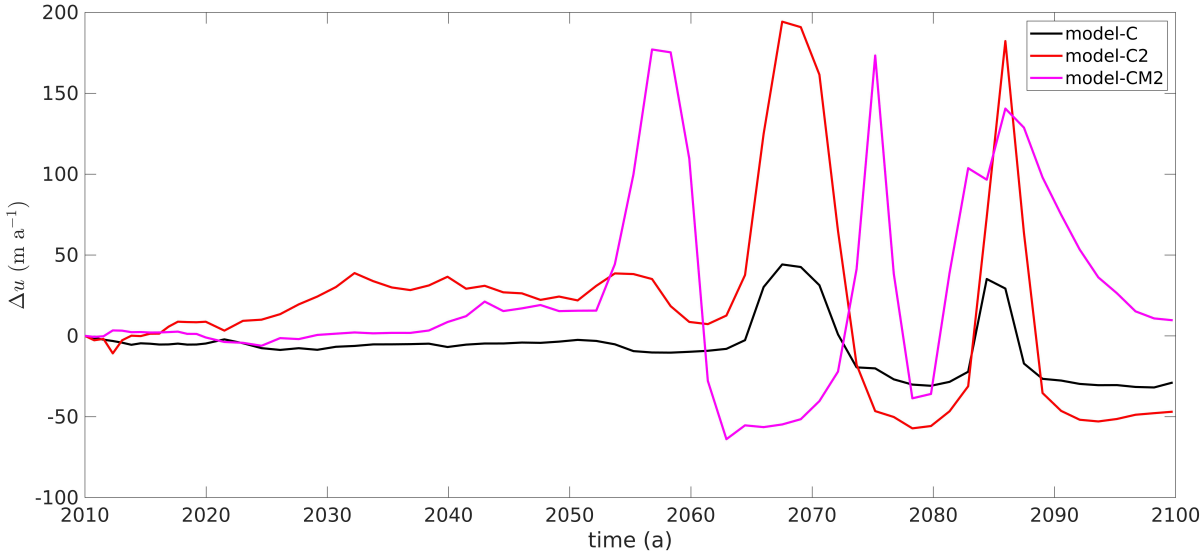


Figure S2. Timeseries of ice speed change in Ice Stream B for Model-C, Model-C2, and Model-CM2.

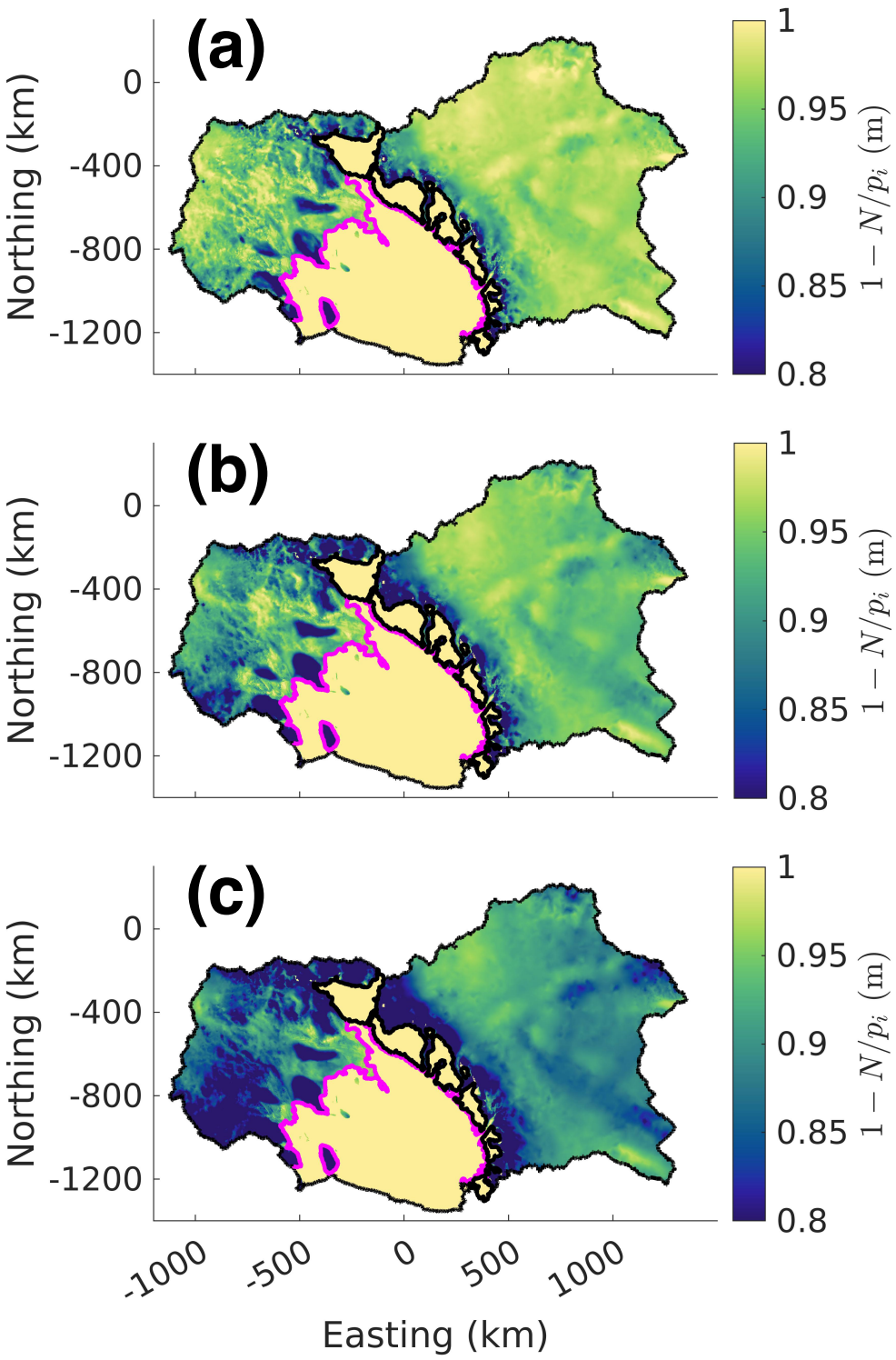


Figure S3. Flotation fraction for steady-state hydrology models with various sheet conductivities, **(a)** $k_s = 10^{-4}\,\mathrm{m}^{7/4}\,\mathrm{kg}^{-1/2}$, **(b)** $k_s = 10^{-3}\,\mathrm{m}^{7/4}\,\mathrm{kg}^{-1/2}$, and **(c)** $k_s = 5 \cdot 10^{-3}\,\mathrm{m}^{7/4}\,\mathrm{kg}^{-1/2}$.

Table S1. Table of relevant model parameters.

Parameter	variable	Value	Units
Sheet parameters			
Bedrock bump height	h_r	0.08	m
Cavity spacing	ℓ_r	2	m
Englacial void ratio	e_ν	10^{-5}	
Exponential fill exponent	γ	ln(10)	
First sheet flow exponent	α_s	5/4	
Second sheet flow exponent	β_s	3/2	
Sheet conductivity	k_s	10^{-3}	$\mathrm{m}^{7/4}\,\mathrm{kg}^{-1/2}$
Start exponential fill thickness	h_c	100, 10	m
Channel parameters			
Channel conductivity	k_c	$5 \cdot 10^{-2}$	$\mathrm{m}^{3/2}\,\mathrm{kg}^{-1/2}$
First channel flow exponent	α_c	5/4	
Maximum channel area		500	m^2
Pressure melt coefficient	c_t	$7.5 \cdot 10^{-8}$	$\mathrm{K\,Pa}^{-1}$
Second channel flow exponent	β_c	3/2	
Sheet width below channel	ℓ_c	2	m
Friction parameters			
Coupling strength constant	ζ	10^7, $2 \cdot 10^7$	$\mathrm{m}^{-4}\,\mathrm{kg\,s}$
Friction exponent	m	1/3	
Shared parameters			
Freshwater density	ρ_{fw}	1000	$\mathrm{kg\,m}^{-3}$
Glen's flow constant	n	3	
Gravitational acceleration	g	9.81	$\mathrm{m\,s}^{-2}$
Ice density	ρ_i	910	$\mathrm{kg\,m}^{-3}$
Ice flow constant in GlaDS	A	$2.5 \cdot 10^{-25}$	$\mathrm{Pa}^3\,\mathrm{s}^{-1}$
Saltwater density	ρ_w	1023	$\mathrm{kg\,m}^{-3}$